ORIGINAL ARTICLE
Electrica 2024; 24(1): 51-59

Fluorescence Microscopy Denoizing via Neighbor Linear Embedding

Cagatay Kirmiziay, Burhan Aydeniz, Mehmet Turkan

Department of Electrical and Electronics Engineering, Izmir University of Economics Faculty of Engineering, Izmir, Turkey

Cite this article as: C. Kirmiziay, B. Aydeniz and M. Turkan, "Fluorescence microscopy denoizing via neighbor linear embedding," *Electrica*, 24(1), 51-59, 2024.

ABSTRACT

One of the difficulties in studying fluorescence imaging of biological structures is the presence of noise corruption. Even though hardware- and software-related technologies have undergone continual improvement, the unavoidable effect of Poisson–Gaussian mixture type is generally encountered in fluorescence microscopy images. This noise should be mitigated to allow the extraction of valuable information from fluorescence images for various types of biological analysis. Thus, this study introduces a new and efficient learning-based denoizing approach for fluorescence microscopy. The proposed approach is based mainly on linear transformations between noise-free and noisy submanifold structures of patch spaces, benefiting from linear neighbor embeddings of local image patches. According to visual and statistical results, the developed algorithm called "neighbor linear-embedding denoizing" algorithm has a highly competitive and generally superior performance in comparison with the other algorithms used for fluorescence microscopy image denoizing in the literature.

Index Terms—Denoizing, fluorescence microscopy, linear embedding, neighbor linear embedding.

I. INTRODUCTION

Using light microscopes, fluorescence microscopy is one of the most feasible techniques for analyzing very small-scale biological specimens. It provides imaging, detection, analysis, and quantification of biological structures, including molecules within subcellular parts; however, the captured images are often corrupted by noise, generally caused by environmental factors and/or imaging equipment. As in all imaging systems, noise corruption is the main reason for quality degradation in the captured images. Even though the exact noise type and level cannot always be estimated, it is known that Poisson–Gaussian mixture generally exists in fluorescence microscopy systems [1, 2]. This noise model for fluorescence microscopy images consists of two types of noise: Poisson noise, which results from signal-dependent uncertainty such as shot noise, and Gaussian noise, which results from signal-independent uncertainty such as thermal noise. To reduce the noise level, one can increase the excitation power of the laser or lamp, as well as the imaging duration [3, 4]. However, this needs great care to avoid damaging the biological structures and to prevent saturation of the fluorescence. Additionally, in real-time and dynamic cases, it is important to capture the images within milliseconds to avoid any imaging-related damage caused by prolonged exposure. Therefore, image denoizing techniques provide viable alternative solutions which are unaffected by these drawbacks associated with exposure time and experimental settings. Poisson–Gaussian denoizing can improve the quality and clarity of fluorescence microscopy images and are particularly valuable in applications needing high-quality images, such as cell biology and neuroscience.

In [4], the fluorescence microscopy denoizing (FMD) dataset is used for analyzing conventional image-processing techniques and deep-learning denoizing models. The FMD dataset contains real fluorescence images, which are corrupted with Poisson–Gaussian noise of 1) confocal microscopy, which uses laser light to stimulate a specimen within a narrow plane, 2) two-photon microscopy, which uses double light wavelengths to excite the fluorescence, and (3) widefield microscopy that captures images of samples under a specific wavelength illumination. In this study, variance stabilizing transformation (VST) [2] is utilized as the initial step to represent Poisson–Gaussian noise under the assumption that it has a unitary variance, similar to Gaussian noise. Subsequently, several image denoizing algorithms are applied to eliminate the unified Gaussian noise. These algorithms include non-local means (NLM) [5], which is grounded on a non-local weighted averaging of pixels in the image, block-matching and 3D filtering (BM3D)

A short version of this study was presented in the 2022 Medical Technologies Congress (TIPTEKNO'22), Antalya, Turkey.

Corresponding author:
Mehmet Turkan

E-mail:
mehmet.turkan@ieu.edu.tr

Received: March 25, 2023

Revision Requested: May 2, 2023

Accepted: July 14, 2023

Publication Date: January 31, 2024

DOI: 10.5152/electrica.2024.23027

[6], which relies on processing similar 2D patches as 3D patch arrays in the transform domain via sparsity constraints, K singular value decomposition (K-SVD) [7], which builds upon dictionary learning schemes via redundant and sparse representations, expected patch log likelihood (EPLL) [8], which considers a patch-based framework based on maximum a posteriori estimation on image patches, and weighted nuclear norm minimization (WNNM) [9], which proposes an iterative algorithm by exploiting image non-local self-similarities. In addition to these methods, Poisson unbiased risk estimate–linear expansion of thresholds (PURE-LET) [10] can be applied as a transform-domain thresholding algorithm designed specifically for the mixed Poisson–Gaussian noise. Hence, VST is not combined with the PURE-LET algorithm. In addition, state-of-the-art deep-learning models have been applied on the same dataset, such as denoizing convolutional neural network (DnCNN) [11], which aims at denoizing unknown noise levels through residual learning and Noise2Noise [12], which has the advantage of being able to function without clean images for training. Despite the statistical and visual success of traditional denoizing techniques, deep-learning methods demonstrate superiority due to their ability to learn intricate patterns and representations from the training data. However, it is important to note here that the choice of a denoizing method strictly depends on the specific problem and the data at hand, and, in some cases, conventional methods may be preferable.

This study elaborates a novel patch-based image denoizing technique for images degraded by the mixed Poisson–Gaussian noise in fluorescence microscopy [13]. The proposed technique, called NLED, builds upon relationships between clean (noise-free) and noisy patches through intrinsic geometric linear transformations of image patch spaces. The experimental results demonstrate that NLED outperforms several other denoizing methods, including NLM, BM3D, K-SVD, EPLL, WNNM, and PURE-LET, when applied either on its own or in combination with VST. Neighbor linear-embedding denoizing is therefore an effective alternative to the existing denoizing algorithms in the literature. This paper is organized as follows. The developed method is technically explained in Section II. The experimental setup and statistical and visual results are presented in Section III. Finally, a brief conclusion and possible future directions are discussed in Section IV.

II. NEIGHBOR LINEAR-EMBEDDING DENOIZING

A. Background

The ultimate objective of a denoizing procedure is to effectively remove the corrupted noise from an image and to estimate the noise-free image as precisely as possible. Fundamentally, the aim is to optimize the intensity-based minimization in (1) as,

$$min\ || \mathbf{X} - \hat{\mathbf{X}} ||_F^2 \quad (1)$$

where $\mathbf{X}$ and $\hat{\mathbf{X}}$ represent the true noise-free image and the predicted image, respectively, and F stands for the Frobenius norm. In general, the clean image $\mathbf{X}$ is not readily available but a noisy version $\mathbf{Y}$ of $\mathbf{X}$ is observed.

The optimization defined in (1) is extremely difficult to solve because of the enormous number of pixels as unknown variables. Hence, there are approximate solutions which reduce the problem to the dimensionality of local image patches, e.g., NLM, BM3D, and K-SVD. Such algorithms reveal the meaningful connections between noisy image patches and their local neighbors or between paired noise-free and noisy sets of image patches. Additionally, these relationships are generally constrained with a sparsity constraint to ensure that the noise is suppressed. Finally, the processed image patches usually overlap with each other to provide local smoothness via averaging in the overlapped regions and hence increase the denoizing performance and prevent blocking or seaming artifacts.

B. Neighbor Linear-Embedding Denoizing

1) Training Phase:

Neighbor linear-embedding denoizing is a patch-based denoizing technique that aims to disclose intrinsic geometric connections between locally linear manifolds [14] of noise-free and noisy patch spaces via linear transformations. Assume that noise-free and noisy sets of images are available for training, the initial step is to calculate the intrinsic properties of the noisy manifold structure from noisy image patches according to (2) as,

$$\underset{\beta_{ik}}{argmin} \left\| \mathbf{y}_i^{tr} - \sum_k \beta_{ik} \tilde{\mathbf{y}}_{ik}^{tr} \right\|_2^2 s.t. \quad \mathbf{1}^T \beta_i = 1 \wedge 0 \le \beta_i \le 1 \quad (2)$$

where $\mathbf{y}_i^{tr}$ and $\tilde{\mathbf{y}}_i^{tr}$ stand for the ith noisy patch for training, $i = 1...I$, and its kth similar neighbor (K-NN) in the same image by minimizing the Euclidean distance, $k = 1...K$, respectively. The size of all image patches is ($n \times n$)-pixels, which are stacked as column-vectors of size $\boldsymbol{n}^2 \times 1$. $\mathbf{1}$ expresses a K-dimensional column-vector of ones, and β_i is a K-dimensional weight vector, i.e., column-vector of optimum reconstruction weights β_{ik}. The calculated reconstruction weights in β_i, $\forall_i$, describe the local geometric properties of the noisy manifold structure. A matrix **B** of size $K \times I$ is constructed from $\beta_i, \forall_i$.

In (2), the optimization is solved with two constraints. The first constraint, $\mathbf{1}^T \beta_i = 1$, assures the estimation of $\mathbf{y}_i^{tr}$ to be in the subspace spanned by its K-NN. The second, $0 \le \beta_i \le 1$, enforces the approximation of $\mathbf{y}_i^{tr}$ to lie in a restricted boundary specified by the utilized K-NN patches. It is worth noting here that there is an additional, but implicit, sparsity notion in the optimization due to the usage of K number of patches, which enables maximum noise rejection.

The second step is to structure the geometry of the co-located clean patch space through the chosen noisy neighbors with respect to (3) as,

$$\underset{\alpha_{ik}}{argmin} \left\| \mathbf{x}_i^{tr} - \sum_k \alpha_{ik} \tilde{\mathbf{y}}_{ik}^{tr} \right\|_2^2 s.t. \quad \mathbf{1}^T \alpha_i = 1 \wedge 0 \le \alpha_i \le 1 \quad (3)$$

where $\mathbf{x}_i^{tr}$ denotes the ith clean patch (co-located with $\mathbf{y}_i^{tr}$) in the training noise-free image. α_i is the K-dimensional column-vector of optimum reconstruction weights α_{ik}. Here, the reconstruction weights in $\alpha_i, \forall_i$, serve to structure the local geometry of the clean manifold with respect to noisy local neighborhood. A matrix **A** of size $K \times I$ is constructed from $\alpha_i, \forall_i$.

Finally, a linear transformation matrix **T** relating the linearized noisy and noise-free patch spaces is obtained by solving a straightforward least-squares optimization as $\mathbf{T} = \mathbf{A}\mathbf{B}^{\dagger}$, where $\mathbf{B}^{\dagger}$ designates the pseudo-inverse of **B**.

2) Test Phase:
After obtaining the transformation **T** from the training dataset, it is applied to each noisy patch $\mathbf{y}_j, \forall_j$, of a given noisy test image **Y** as follows. First, *K*-NN set of patches $\{\tilde{\mathbf{y}}_{jk}\}$ for $\mathbf{y}_j$ is extracted from **Y** and the optimum weight vector β_j is calculated via (2). Second, this vector is transformed to $\alpha_j \approx \mathbf{T}\beta_j$ to predict the intrinsic manifold structure of the noise-free patch space. Last, the denoized output $\hat{\mathbf{x}}_j$ is calculated in (4) as,

$$\hat{\mathbf{x}}_j = \sum_k \alpha_{jk}\tilde{\mathbf{y}}_{jk}. \quad (4)$$

A final denoized image $\hat{\mathbf{X}}$ is generated by spatially relocating the estimated patches $\hat{\mathbf{x}}_j, \forall_j$, in $\hat{\mathbf{X}}$. There are overlaps between these patches, and the multiple-predicted pixel values are uniformly averaged in the overlapping regions. The proposed NLED algorithm is detailed in Algorithm 1.

C. Variance Stabilizing Transformation + Neighbor Linear-Embedding Denoizing

Neighbor linear-embedding denoizing is combined with Anscombe VST resulting in a version called VST+NLED. The VST+NLED algorithm is given in Algorithm 2.

Algorithm 1: Neighbor linear-embedding denoizing algorithm
Training Phase
Input: Coupled set of noisy and clean images
Output: Transformation matrix **T**
for *each coupled patch pair* $\mathbf{y}_i^{tr}$ *and* $\mathbf{x}_i^{tr}$ **do**
Find *K*-NN set for $\mathbf{y}_i^{tr}$
Optimize (2) to obtain β_i
Optimize (3) to obtain $\boldsymbol{a}_i$
End
Construct structure matrices **A** and **B**
Calculate $\mathbf{T} = \mathbf{AB}^{\dagger}$
Test Phase
Input: Noisy test image **Y**, and **T**
Output: Denoized image $\hat{\mathbf{X}}$
Extract all patches $\mathbf{y}_j$ of **Y**
for *each* $\boldsymbol{y}_j$ **do**
Find *K*-NN set for $\mathbf{y}_j$
Optimize Eq. (2) to obtain β_j
Apply the transformation $\boldsymbol{a}_j \approx \mathbf{T}\boldsymbol{\beta}_j$
Estimate $\hat{\mathbf{x}}_j$ via (4)
end
Reconstruct $\hat{\mathbf{X}} \leftarrow \{\hat{\mathbf{x}}_j\}$ via averaging

III. EXPERIMENTAL SETUP AND RESULTS

A. Dataset

This study utilizes the FMD dataset (publicly available online [15]), which comprises real fluorescence microscopy images contaminated by Poisson–Gaussian noise. The dataset includes 12 subjects, and each subject has 20 field of views (FOVs) with 50 raw images, resulting in a total of 12 000 images. These images feature various biological samples such as cells, zebrafish, and mouse brain tissues captured by different types of microscopes, including commercial confocal, two-photon, and widefield microscopes. To produce ground truth images, the raw images for each FOV are simply averaged. Additionally, noisy images with different levels of noise are obtained by averaging different numbers of raw images (2, 4, 8, 16), resulting in a total of 60 000 noisy images.

For training, three distinct datasets are extracted from the FMD dataset. The first dataset, called MICE, comprises 12 two-photon microscopy mouse brain images chosen from the first frames of the first 12 FOVs. The second dataset, called ZEBRA, consists of 12 confocal microscopy zebrafish embryo images selected from the first frames of the first 12 FOVs. The third dataset, named MICE+ZEBRA, contains a mix of six two-photon and six confocal microscopy images from the first frames of their first six FOVs, respectively. Additionally, to assess and compare the denoizing performance, a mixed test dataset was generated, consisting of 48 images randomly selected from the 19th FOV of all 12 subjects, with four frames per image. This dataset comprises confocal microscopy, which includes Bovine Pulmonary Artery Endothelial Cells (BPAE) (nuclei, F-actin, and Mito), zebrafish, and mouse brain samples, two-photon microscopy, which includes BPAE (nuclei, F-actin, and Mito) and mouse brain samples, and widefield microscopy, which includes BPAE (nuclei, F-actin, Mito) samples. Note here that the BPAE (nuclei, F-actin, and Mito) image samples are not included in any training sets.

Algorithm 2: VST + NLED algorithm
Training Phase
Input: Coupled set of noisy and clean images
Output: Transformation matrix **T**
Noisy images $\leftarrow$ VST (noisy images)
for *each coupled patch pair* $\mathbf{y}_i^{tr}$ *and* $\mathbf{x}_i^{tr}$ **do**
Find *K*-NN set for $\mathbf{y}_i^{tr}$
Optimize (2) to obtain β_i
Optimize (3) to obtain $\boldsymbol{a}_i$
End
Construct structure matrices **A** and **B**
Calculate $\mathbf{T} = \mathbf{AB}^{\dagger}$
Test Phase

TABLE I. MULTI-PASS NLED DENOIZING PERFORMANCE ON THE MIXED TEST SET

Mixed Set		**Noisy Input**	**Pass-1**	**Pass-2**	**Pass-3**
Method	**Training dataset**	**PSNR/SSIM**	**PSNR/SSIM**	**PSNR/SSIM**	**PSNR/SSIM**
NLED	MICE	27.22/0.5442	32.33/0.8595	32.82/0.8742	32.83/0.8777
NLED	ZEBRA	27.22/0.5442	32.40/0.8655	32.65/0.8812	32.49/0.8839
NLED	MICE+ZEBRA	27.22/0.5442	32.39/0.8639	32.72/0.8797	32.63/0.8834
VST+NLED	MICE	27.22/0.5442	32.39/0.8608	32.87/0.8758	**32.90/**0.8794
VST+NLED	ZEBRA	27.22/0.5442	32.46/0.8673	32.69/0.8829	32.50/**0.8853**
VST+NLED	MICE+ZEBRA	27.22/0.5442	32.45/0.8656	32.78/0.8807	32.68/0.8845

NLED, neighbor linear-embedding denoizing; PSNR, peak signal-to-noise ratio; SSIM, structural similarity index measure; VST, variance stabilizing transformation.

TABLE II. MULTI-PASS NLED DENOIZING PERFORMANCE ON TWO-PHOTON MICROSCOPY IMAGES

Two-photon			**Noisy Input**	**Pass-1**	**Pass-2**	**Pass-3**
Sample	**Method**	**Training Dataset**	**PSNR/SSIM**	**PSNR/SSIM**	**PSNR/SSIM**	**PSNR/SSIM**
BPAE (nuclei)	NLED	MICE	24.24/0.7166	29.79/0.9239	30.56/0.9559	30.62/0.9608
	NLED	ZEBRA	24.24/0.7166	29.86/0.9275	30.42/0.9555	30.33/0.9575
	NLED	MICE+ZEBRA	24.24/0.7166	29.84/0.9264	30.47/0.9557	30.44/0.9587
	VST+NLED	MICE	24.24/0.7166	29.83/0.9248	30.61/0.9569	**30.68/0.9619**
	VST+NLED	ZEBRA	24.24/0.7166	29.91/0.9290	30.46/0.9566	30.36/0.9582
	VST+NLED	MICE+ZEBRA	24.24/0.7166	29.89/0.9278	30.52/0.9569	30.49/0.9598
BPAE (F-actin)	NLED	MICE	25.30/0.7727	31.31/0.8719	31.69/0.8567	31.57/0.8489
	NLED	ZEBRA	25.30/0.7727	31.28/0.8691	31.33/0.8458	30.94/0.8269
	NLED	MICE+ZEBRA	25.30/0.7727	31.30/0.8700	31.45/0.8494	31.15/0.8348
	VST+NLED	MICE	25.30/0.7727	31.37/**0.8722**	**31.76/**0.8569	31.63/0.8491
	VST+NLED	ZEBRA	25.30/0.7727	31.35/0.8691	31.36/0.8447	30.95/0.8247
	VST+NLED	MICE+ZEBRA	25.30/0.7727	31.36/0.8700	31.51/0.8494	31.22/0.8351
BPAE (Mito)	NLED	MICE	30.85/0.8771	36.44/0.9351	36.77/0.9279	36.60/0.9230
	NLED	ZEBRA	30.85/0.8771	36.35/0.9325	36.28/0.9197	35.84/0.9090
	NLED	MICE+ZEBRA	30.85/0.8771	36.38/0.9333	36.44/0.9224	36.09/0.9138
	VST+NLED	MICE	30.85/0.8771	36.57/**0.9366**	**36.93/**0.9295	36.75/0.9246
	VST+NLED	ZEBRA	30.85/0.8771	36.50/0.9340	36.39/0.9207	35.92/0.9092
	VST+NLED	MICE+ZEBRA	30.85/0.8771	36.53/0.9348	36.59/0.9240	36.23/0.9153
Mouse brain	NLED	MICE	24.87/0.6650	31.86/0.9100	33.33/0.9555	33.41/0.9624
	NLED	ZEBRA	24.87/0.6650	31.85/0.9146	32.62/0.9548	32.15/0.9574
	NLED	MICE+ZEBRA	24.87/0.6650	31.86/0.9132	32.86/0.9552	32.56/0.9593
	VST+NLED	MICE	24.87/0.6650	31.88/0.9104	33.36/0.9558	**33.44/0.9626**
	VST+NLED	ZEBRA	24.87/0.6650	31.88/0.9155	32.59/0.9551	32.07/0.9571
	VST+NLED	MICE+ZEBRA	24.87/0.6650	31.90/0.9141	32.92/0.9557	32.63/0.9597

NLED, neighbor linear-embedding denoizing; PSNR, peak signal-to-noise ratio; SSIM, structural similarity index measure; VST, variance stabilizing transformation.

TABLE III. MULTI-PASS NLED DENOIZING PERFORMANCE ON CONFOCAL MICROSCOPY IMAGES

Confocal			**Noisy Input**	**Pass-1**	**Pass-2**	**Pass-3**
Sample	**Method**	**Training Dataset**	**PSNR/SSIM**	**PSNR/SSIM**	**PSNR/SSIM**	**PSNR/SSIM**
BPAE (nuclei)	NLED	MICE	31.99/0.9534	37.40/0.9802	37.40/0.9795	37.30/0.9786
	NLED	ZEBRA	31.99/0.9534	37.22/0.9786	36.63/0.9746	36.09/0.9713
	NLED	MICE+ZEBRA	31.99/0.9534	37.29/0.9791	36.89/0.9762	36.49/0.9738
	VST+NLED	MICE	31.99/0.9534	37.45/0.9822	**37.49**/**0.9831**	37.40/0.9828
	VST+NLED	ZEBRA	31.99/0.9534	37.28/0.9810	36.66/0.9781	36.09/0.9748
	VST+NLED	MICE+ZEBRA	31.99/0.9534	37.34/0.9813	37.03/0.9802	36.64/0.9781
BPAE (F-actin)	NLED	MICE	28.43/0.8952	32.29/0.9180	32.04/0.9058	31.93/0.9027
	NLED	ZEBRA	28.43/0.8952	31.96/0.9115	31.16/0.8861	30.62/0.8679
	NLED	MICE+ZEBRA	28.43/0.8952	32.07/0.9136	31.44/0.8927	31.03/0.8801
	VST+NLED	MICE	28.43/0.8952	**32.36**/**0.9187**	32.09/0.9062	31.99/0.9032
	VST+NLED	ZEBRA	28.43/0.8952	32.00/0.9115	31.15/0.8848	30.58/0.8650
	VST+NLED	MICE+ZEBRA	28.43/0.8952	32.11/0.9137	31.54/0.8941	31.13/0.8817
BPAE (Mito)	NLED	MICE	33.00/0.9529	36.69/0.9610	35.97/0.9530	35.62/0.9488
	NLED	ZEBRA	33.00/0.9529	36.23/0.9549	34.85/0.9365	34.04/0.9219
	NLED	MICE+ZEBRA	33.00/0.9529	36.38/0.9569	35.19/0.9419	34.51/0.9311
	VST+NLED	MICE	33.00/0.9529	**36.76**/**0.9633**	36.02/0.9555	35.67/0.9514
	VST+NLED	ZEBRA	33.00/0.9529	36.26/0.9573	34.80/0.9381	33.95/0.9224
	VST+NLED	MICE+ZEBRA	33.00/0.9529	36.42/0.9591	35.28/0.9455	34.60/0.9347
Zebrafish embryo	NLED	MICE	22.86/0.7504	28.89/0.8773	29.61/0.8827	29.60/0.8810
	NLED	ZEBRA	22.86/0.7504	28.77/0.8714	29.01/0.8639	28.72/0.8546
	NLED	MICE+ZEBRA	22.86/0.7504	28.82/0.8738	29.20/0.8700	29.00/0.8631
	VST+NLED	MICE	22.86/0.7504	28.97/0.8808	**29.70**/**0.8873**	**29.70/**0.8863
	VST+NLED	ZEBRA	22.86/0.7504	28.82/0.8740	29.01/0.8656	28.69/0.8557
	VST+NLED	MICE+ZEBRA	22.86/0.7504	28.88/0.8766	29.24/0.8733	29.05/0.8668
Mouse brain	NLED	MICE	29.36/0.9000	36.01/0.9709	36.36/0.9765	36.14/0.9764
	NLED	ZEBRA	29.36/0.9000	35.85/0.9704	35.49/0.9730	34.74/0.9700
	NLED	MICE+ZEBRA	29.36/0.9000	35.90/0.9706	35.76/0.9742	35.18/0.9722
	VST+NLED	MICE	29.36/0.9000	36.14/0.9721	**36.50**/**0.9779**	36.27/0.9778
	VST+NLED	ZEBRA	29.36/0.9000	35.96/0.9718	35.52/0.9743	34.72/0.9710
	VST+NLED	MICE+ZEBRA	29.36/0.9000	36.02/0.9720	35.92/0.9758	35.29/0.9738

NLED, neighbor linear-embedding denoizing; PSNR, peak signal-to-noise ratio; SSIM, structural similarity index measure; VST, variance stabilizing transformation.

Input: Noisy test image $\mathbf{Y}$, and $\mathbf{T}$
Output: Denoized image $\hat{\mathbf{X}}$

$\mathbf{Y} \leftarrow \mathrm{VST}(\mathbf{Y})$
Extract all patches $\mathbf{y}_j$ of $\mathbf{Y}$

TABLE IV. MULTI-PASS NLED DENOIZING PERFORMANCE ON WIDEFIELD MICROSCOPY IMAGES

Widefield			**Noisy Input**	**Pass-1**	**Pass-2**	**Pass-3**
Sample	**Method**	**Training Dataset**	**PSNR/SSIM**	**PSNR/SSIM**	**PSNR/SSIM**	**PSNR/SSIM**
BPAE (nuclei)	NLED	MICE	25.58/0.4702	29.36/0.6412	30.17/0.6819	30.48/0.6985
	NLED	ZEBRA	25.58/0.4702	30.11/0.6743	31.54/0.7439	**32.38/**0.7809
	NLED	MICE+ZEBRA	25.58/0.4702	29.90/0.6648	31.17/0.7269	31.81/0.7591
	VST+NLED	MICE	25.58/0.4702	29.36/0.6420	30.18/0.6833	30.48/0.6995
	VST+NLED	ZEBRA	25.58/0.4702	30.17/0.6776	31.62/0.7487	**32.38/0.7865**
	VST+NLED	MICE+ZEBRA	25.58/0.4702	29.95/0.6678	31.11/0.7250	31.75/0.7570
BPAE (F-actin)	NLED	MICE	23.88/0.4747	28.19/0.6512	29.37/0.7022	29.83/0.7230
	NLED	ZEBRA	23.88/0.4747	28.87/0.6788	30.71/0.7552	31.63/0.7925
	NLED	MICE+ZEBRA	23.88/0.4747	28.67/0.6708	30.36/0.7410	31.20/0.7754
	VST+NLED	MICE	23.88/0.4747	28.21/0.6520	29.40/0.7036	29.86/0.7240
	VST+NLED	ZEBRA	23.88/0.4747	28.94/0.6819	30.83/0.7598	**31.76**/**0.7971**
	VST+NLED	MICE+ZEBRA	23.88/0.4747	28.75/0.6738	30.33/0.7398	31.16/0.7739
BPAE (Mito)	NLED	MICE	26.23/0.5114	29.76/0.6735	30.56/0.7127	30.88/0.7287
	NLED	ZEBRA	26.23/0.5114	30.43/0.7019	31.77/0.7648	32.46/0.7974
	NLED	MICE+ZEBRA	26.23/0.5114	30.24/0.6937	31.45/0.7507	32.06/0.7796
	VST+NLED	MICE	26.23/0.5114	29.77/0.6742	30.58/0.7139	30.89/0.7295
	VST+NLED	ZEBRA	26.23/0.5114	30.48/0.7046	31.86/0.7689	**32.57**/**0.8022**
	VST+NLED	MICE+ZEBRA	26.23/0.5114	30.29/0.6963	31.41/0.7492	32.02/0.7781

NLED, neighbor linear-embedding denoizing; PSNR, peak signal-to-noise ratio; SSIM, structural similarity index measure; VST, variance stabilizing transformation.

for *each* $\mathbf{y}_j$ **do**
Find *K*-NN set for $\mathbf{y}_j$
Optimize (2) to obtain $\boldsymbol{\beta}_j$
Apply the transformation $\boldsymbol{a}_j \approx \mathbf{T}\boldsymbol{\beta}_j$
Estimate $\hat{\mathbf{x}}_j$ via (4)
End
Reconstruct $\hat{\mathbf{X}} \leftarrow \{\hat{\mathbf{x}}_j\}$ via averaging

NLED, neighbor linear-embedding denoizing; VST, variance stabilizing transformation.

B. Experimental Setup

To ensure scale invariance, a multiscale model of NLED is trained using the three training datasets. This is achieved by obtaining rescaled versions of coupled clean and noisy images, which are downsampled with factors of 0.9, 0.8, 0.75, 0.5, and 0.25. These rescaled images are included in the patch-pair extraction process during the training phase.

A refinement approach is proposed to improve the current denoizing solution and account for the possibility of suboptimal optimizations and the final patch-averaging operation. As a straightforward extension, the main algorithm of NLED in Algorithm 1 and VST+NLED in Algorithm 2 are adapted into a multi-pass scheme. In this scheme, the denoizing outputs obtained from the previous pass are used as the inputs for the following pass, and the same algorithm is applied in each. This method involves multiple passes to refine the learned transformations during both training and test phases. This iterative process aims to improve the denoizing solution and reduce suboptimal optimizations and patch-averaging errors. It is worth noting that VST is only employed in the first pass of Algorithm 2, while subsequent passes use the outputs of the previous pass as inputs.

C. Experimental Results and Discussion

Statistical and visual comparisons are given in this section to evaluate the performance of the proposed denoizing algorithm. All experiments are carried out with patch size of 9×9 pixels and the number of neighbors $K = 16$. The parameters are analyzed in terms of the content of the training dataset, the number of passes, and the effect of the additional VST algorithm. Table I reports the statistical results of NLED and VST+NLED on the mixed test dataset in terms of peak signal-to-noise ratio (PSNR) and structural similarity index measure (SSIM). These statistics show that VST makes a contribution to the obtained results, but it is less significant than the content of the training dataset and the multi-pass strategy. In terms of PSNR, the best test performance is achieved with VST+NLED using the MICE training set.

TABLE V. STATISTICAL COMPARISON WITH THE BENCHMARK METHODS

	Method	PSNR	SSIM
	Noisy Input	27.22	0.5442
	VST+NLM	31.25	0.7503
	VST+BM3D	32.71	0.7922
	VST+K-SVD	32.02	0.7746
	VST+K-SVD(D) (DCT dictionary)	31.77	0.7712
	VST+K-SVD(G) (global dictionary)	31.98	0.7752
	VST+EPLL	32.61	0.7876
	VST+WNNM	32.52	0.7880
	PURE-LET	31.95	0.7664
	DnCNN	34.88	0.9063
	Noise2Noise	**35.40**	**0.9187**
Proposed	NLED-(MICE)	32.83	0.8777
Proposed	NLED-(ZEBRA)	32.49	0.8839
Proposed	NLED-(MICE+ZEBRA)	32.63	0.8834
Proposed	VST+NLED-(MICE)	**32.90**	0.8794
Proposed	VST+NLED-(ZEBRA)	32.50	**0.8853**
Proposed	VST+NLED-(MICE+ZEBRA)	32.68	0.8845

BM3D, block-matching and 3D filtering; DnCNN, denoizing convolutional neural network; EPLL, expected patch log likelihood; NLED, neighbor linear-embedding denoizing; NLM, non-local means; PURE-LET, Poisson unbiased risk estimate–linear expansion of thresholds; VST, variance stabilizing transformation; WNNM, weighted nuclear norm minimization.

Additionally, Tables II–IV give more detailed statistical performance comparisons for individual biological samples of specific types of microscopy images. As can be clearly seen from these tables, VST+NLED (slightly) improves the statistics when compared to NLED alone. Table II demonstrates statistical comparisons for two-photon microscopy images. In this setup, VST+NLED using MICE is the most successful approach for all biological samples of two-photon images.

Similarly, Table III summarizes statistical results for confocal microscopy images. Of all biological samples, the superior results are obtained with VST+NLED and the MICE training set. Furthermore, according to Table IV, widefield microscopy images can be successfully denoized by VST+NLED with ZEBRA because of the similarity between confocal and widefield microscopy techniques. Note here that the widefield microscopy images are not included in any training sets. Also, the multi-pass approach proved to be very effective in most experiments.

A statistical comparison with the other benchmark algorithms in the literature is given in Table V. Variance stabilizing transformation + neighbor linear-embedding denoizing clearly outperforms VST+NLM, VST+BM3D, VST+K-SVD, VST+KSVD(D) (with an over-complete Discrete cosine transform [DCT] dictionary), VST+KSVD(G) (with a global trained dictionary), VST+EPLL, VST+WNNM, and PURE-LET denoizing systems not only statistically but also visually, as seen in Fig. 1 and Fig. 2. Fig. 1 illustrates an example visual comparison of the denoized zebrafish image from confocal microscopy and Fig. 2 demonstrates the image denoizing results of the colored widefield microscopy. It can be concluded that the developed NLED (and VST+NLED) method has superior statistics in comparison with the other traditional methods, while its performance is potentially competitive against deep-learning architectures, e.g., DnCNN and Noise2Noise.

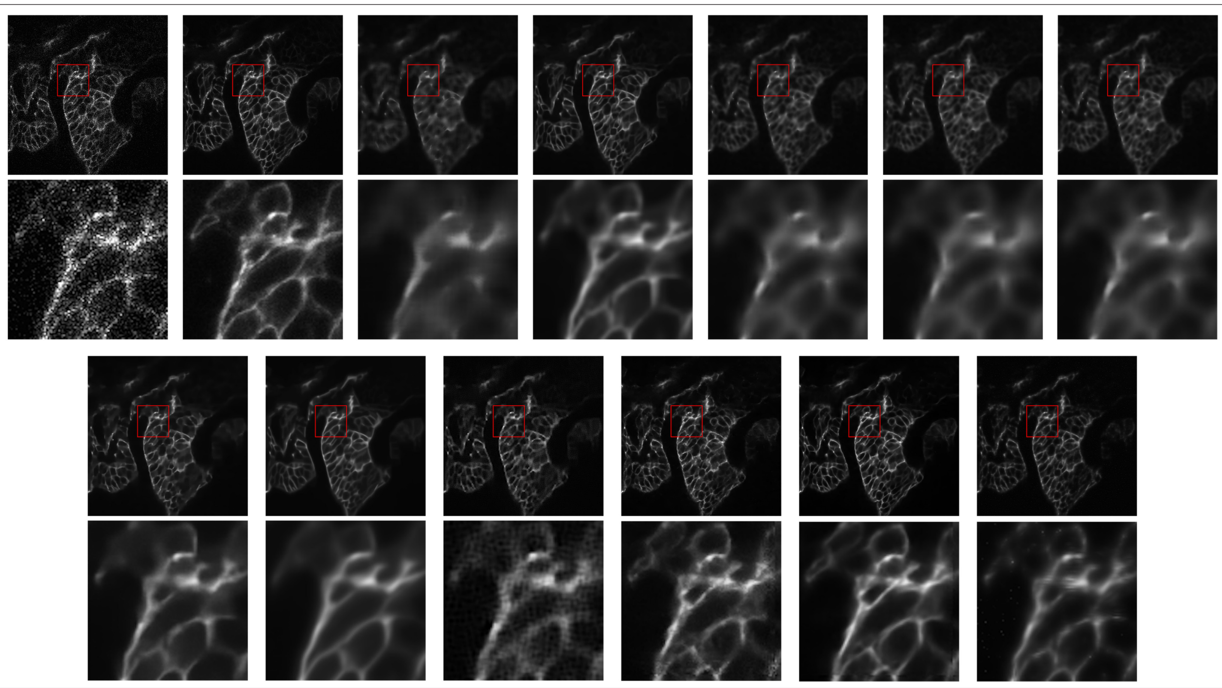

Fig. 1. Visual comparisons of the denoized zebrafish image from confocal microscopy. (Top-two-rows left- to-right) Noisy input, ground truth, VST+NLM, VST+BM3D, VST+K-SVD, VST+K-SVD(D), and VST+K-SVD(G). (Bottom-two-rows left-to-right) VST+EPLL, VST+WNNM, PURE-LET, DnCNN, Noise2Noise, and VST+NLED.

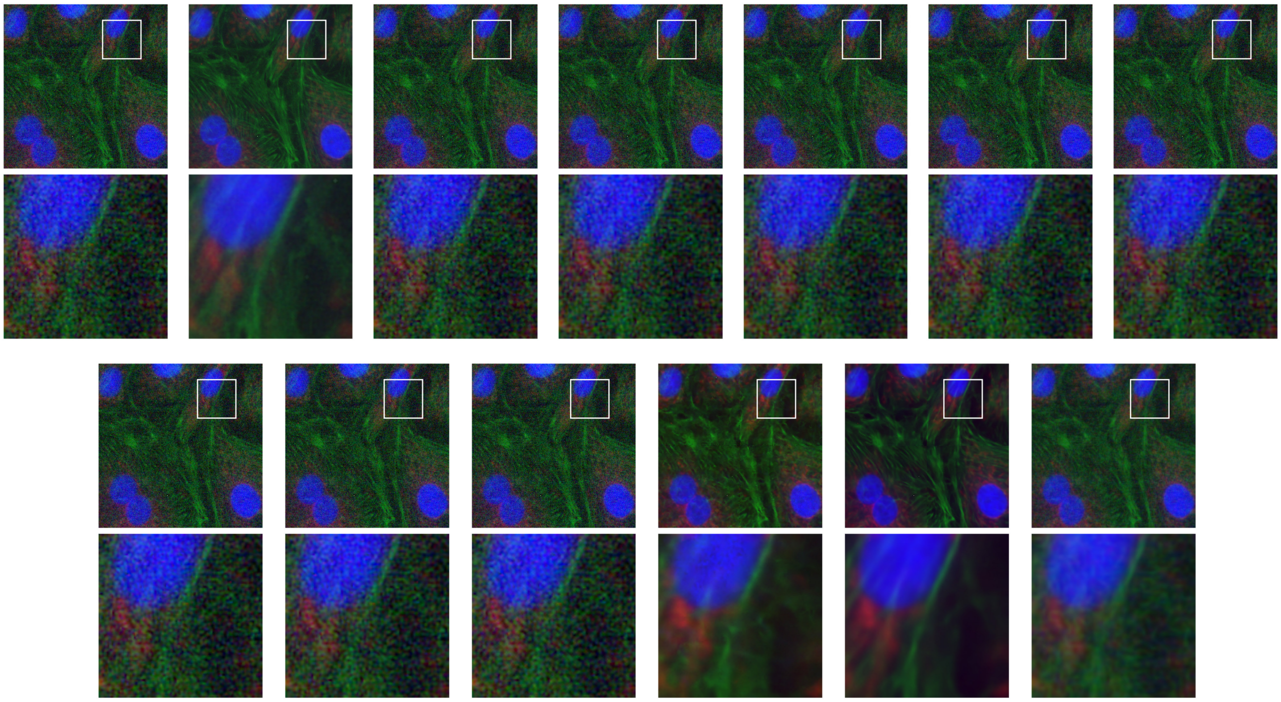

Fig. 2. Visual comparisons of the denoized BPAE image from widefield microscopy. (Top-two-rows left-to- right) Noisy input, ground truth, VST+NLM, VST+BM3D, VST+K-SVD, VST+K-SVD(D), and VST+K-SVD(G). (Bottom-two-rows left-to-right) VST+EPLL, VST+WNNM, PURE-LET, DnCNN, Noise2Noise, and VST+NLED.

IV. CONCLUSION

This study introduces a new and effective method to remove Poisson–Gaussian noise from fluorescence microscopy images using a patch-based approach called NLED. The technique utilizes neighbor linear embeddings to understand the relationship between the geometric properties of clean and noisy patch spaces. In the study, NLED was proven to produce denoizing results often superior to similar benchmark studies in the field. Although not a deep-learning method itself, if it were redesigned in a layered structure, it has the potential to be a strong competitor to those methods. Future research should focus on extending NLED to the area of deep structures.

Peer-review: Externally peer-reviewed.

Author Contributions: Concept – C.K., B.A., M.T.; Design – C.K., B.A., M.T.; Supervision – M.T.; Materials – C.K., B.A.; Data Collection and/or Processing – C.K., B.A.; Analysis and/or Interpretation – C.K., B.A., M.T.; Literature Review – C.K., B.A.; Writing – C.K., B.A.; Critical Review – M.T.

Declaration of Interests: The authors have no conflict of interest to declare.

Funding: The authors declared that this study has received no financial support.

REFERENCES

1. A. Foi, M. Trimeche, V. Katkovnik, and K. Egiazarian, "Practical Poissonian-Gaussian noise modeling and fitting for single-image raw-data," *IEEE Trans. Image Process.*, vol. 17, no. 10, pp. 1737–1754, 2008. [CrossRef]
2. M. Makitalo, and A. Foi, "Optimal inversion of the generalized Anscombe transformation for Poisson- Gaussian noise," *IEEE Trans. Image Process.*, vol. 22, no. 1, pp. 91–103, 2013. [CrossRef]
3. Y. Zhang *et al.*, "Saturation-compensated measurements for fluorescence lifetime imaging microscopy," *Opt. Lett.*, vol. 42, no. 1, pp. 155–158, 2017. [CrossRef]
4. Y. Zhang *et al.*, "A Poisson-Gaussian denoising dataset with real fluorescence microscopy images," IEEE Conf. Comp. Vis. Patt. Recog, pp. 11702–11710, 2019. [CrossRef]
5. A. Buades, B. Coll, and J.-M. Morel, "Non-local means denoising," *Image Process. On Line*, vol. 1, pp. 208–212, 2011. [CrossRef]
6. K. Dabov, A. Foi, V. Katkovnik, and K. Egiazarian, "Image denoising by sparse 3-D transform-domain collaborative filtering," *IEEE Trans. Image Process.*, vol. 16, no. 8, pp. 2080–2095, 2007. [CrossRef]
7. M. Aharon, M. Elad, and A. Bruckstein, "K-SVD: An algorithm for designing overcomplete dictionaries for sparse representation," *IEEE Trans. Signal Process.*, vol. 54, no. 11, pp. 4311–4322, 2006. [CrossRef]
8. D. Zoran, and Y. Weiss, "From learning models of natural image patches to whole image restoration," IEEE Conf. Comp. Vis. Patt. Recog., pp. 479–486, 2011.
9. S. Gu, L. Zhang, W. Zuo, and X. Feng, "Weighted nuclear norm minimization with application to image denoising," IEEE Conf. Comp. Vis. Patt. Recog., pp. 2862–2869, 2014. [CrossRef]
10. F. Luisier, T. Blu, and M. Unser, "Image denoising in mixed Poisson-Gaussian noise," *IEEE Trans. Image Process.*, vol. 20, no. 3, pp. 696–708, 2011. [CrossRef]
11. K. Zhang, W. Zuo, Y. Chen, D. Meng, and L. Zhang, "Beyond a Gaussian denoiser: Residual learning of deep CNN for image denoising," *IEEE Trans. Image Process.*, vol. 26, no. 7, pp. 3142–3155, 2017. [CrossRef]
12. J. Lehtinen *et al.*, "Noise2Noise: Learning image restoration without clean data," *arXiv Preprint ArXiv:1803.04189*, 2018.
13. C. Kirmiziay, B. Aydeniz, and M. Turkan, "NLED: Neighbor linear-embedding denoising for fluorescence microscopy images," *Med. Tech. Congr.*, pp. 1–2, 2022.
14. S. T. Roweis, and L. K. Saul, "Nonlinear dimensionality reduction by locally linear embedding," *Science*, vol. 290, no. 5500, pp. 2323–2326, 2000. [CrossRef]
15. "*Fluorescence Microscopy Denoising (FMD) dataset*". Available: https://github.com/yinhaoz/denoising-fluorescence. [Accessed: 17-05-2023].

Cagatay Kirmiziay received his B.Sc. degree (with high honors) and M.Sc. degree in the department of Electrical and Electronics Engineering from the Izmir University of Economics, Turkey, in 2018 and 2022, respectively. His research interests include image denoizing and biomedical images. He is currently a research assistant at the UMK Institute of Physics in a project studying anterior and posterior images of eye movements.

Burhan Aydeniz received his B.Sc. degree (with honors) and M.Sc. degree in the department of Electrical and Electronics Engineering from the Izmir University of Economics, Turkey, in 2020 and 2023 respectively. His research interests include image enhancement on biomedical and microscopy images, light field super-resolution and computer vision.

Mehmet Turkan received the B.Sc. (Hhons) degree in electrical and electronics engineering from Eskisehir Osmangazi University, Turkey in 2004, received the M.Sc. degree in electrical and electronics engineering from Bilkent University, Turkey in 2007. He received the Ph.D. degree in computer science from Bretagne Atlantique Research Center (INRIA) and University of Rennes 1, France, in 2011. He is currently an Associate Professor of Electrical and Electronics Engineering at the Faculty of Engineering, Izmir University of Economics, Turkey. From January 2013 to July 2015, he was a full-time researcher at Technicolor Research and Innovation Center, France, where he was a post-doctoral researcher between November 2011 and December 2012. He was the recipient of the HUAWEI Best Student Paper Award in the 2010 IEEE International Conference on Image Processing (IEEE-ICIP) and was a nominee for the Best Student Paper Award in the 2011 IEEE-ICIP. His research interests include signal processing with an emphasis on image and video processing, pattern recognition and classification, computer vision, machine learning, and artificial intelligence.